PROCEEDINGS, 50th Workshop on Geothermal Reservoir Engineering
Stanford University, Stanford, California, February 10-12, 2025
SGP-TR-229

Thermal Kaiser effect and Thermo-mechanical response of Utah FORGE granitoid

Xuejun Zhou, Pradeep Gautam, Ahmad Ghassemi

Reservoir Geomechanics and Seismicity Research Group, The University of Oklahoma, Norman, OK, USA

Ahmad.ghassemi@ou.edu

Keywords: Utah FORGE, Granitoid, Thermal Kaiser Effect, Thermal Cycling

ABSTRACT

Understanding the rock response to temperature variations is essential to EGS and superhot resource development. In particular, the impact of heating and cooling on the rock porosity and permeability is pivotal for advancing various core-based techniques used for in-situ stress and poroelastic properties determination, and log data calibration at Utah FORGE. The effects of mechanical cyclic loading and related microcrack development have been relatively well-studied, however, the nature of microcrack development in relation to the heating and cooling processes have not been clearly established. The extent of damage and operating mechanisms induced by thermal cycling remain poorly understood, particularly under stress and pressure conditions. In this paper we present the result of thermal cycling test on Utah FORGE granitoid samples. Granitoid core plugs, from FORGE were subjected to multiple heating and cooling cycles at varying peak temperatures and under a constant stress state resembling their in-situ stress conditions. Wave propagation velocities and acoustic emissions were recorded continuously throughout the thermal cycling process and the former were used to determine dynamic elastic properties. The manner and timing of thermal cracking, AE, and the variation of elastic properties of the rocks demonstrate interesting new phenomena with practical consequences for laboratory investigation of thermal stimulation, stress measurement and log interpretation.

1. INTRODUCTION

The development of Enhanced Geothermal Systems (EGS) and the exploitation of superhot geothermal resources have become increasingly important as global demand for renewable energy rises (Allis et al., 2019; Ghassemi, 2012; Tester et al., 2006). Geothermal reservoirs, particularly those subjected to thermal stimulation, are highly sensitive to temperature fluctuations, which can significantly influence rock properties such as mechanical strength and microstructure. These can in turn impact stimulation mechanisms and outcomes (Hung et al., 2019; Ye and Ghassemi 2018-2020). These changes are critical for optimizing geothermal energy extraction, making a detailed understanding of rock behavior under thermal cycling essential for advancing EGS. The rock mechanical response to thermal perturbations has been the subject of recent studies (Jin et al, 2019). However, often the nature of cracking has not been established in relation to heating and cooling processes.

Thermal cycling, which involves repeated heating and cooling of rocks, induces mechanical stress that can lead to microcrack formation and propagation. These thermal-induced cracks are particularly prevalent in brittle rocks, such as granite, where differential thermal expansion between minerals generates localized internal stresses (Fredrich and Wong, 1986; Tarasov and Ghassemi, 2013). While thermal cycling has been studied extensively, the effects of these cycles on microcrack evolution—especially when combined with mechanical stress—remain less understood (Fredrich and Wong, 1986; Darot et al., 1992). Also, as mentioned before, it is not always apparent if the crack formed during heating or cooling. This requires continuous dynamic measurements and AE recording during the heating and cooling cycles (Daoud et al., 2020; Griffiths et al., 2024). Recent research has started to explore the interaction between thermal cycling and stresses, but the underlying mechanisms of microcrack formation and propagation in these complex environments are still not fully characterized (Griffiths et al., 2018; Ge and Sun, 2018; Reuschle et al., 2006). AE signals, generated by the rapid release of energy due to crack formation and propagation, provide valuable real-time information about the mechanical response of rocks (Obert, 1977; Wang et al., 1989). AE activity has been shown to correlate closely with temperature changes during thermal cycling; the degradation of macro-properties of the rocks is largely attributed to the generation of grain boundary and intra-grain micro-cracks inside the rock specimens due to the applied thermal stress (Rong et al., 2018). This makes AE monitoring an essential tool for tracking damage progression and understanding rock failure mechanisms in geothermal systems. For example, Ge and Sun (2018) and Bu et al. (2024) recorded AE in uniaxially loaded samples subjected to heating and cooling and noted microcrack initiation in granite during thermal cycling. These studies observed increased AE during temperature ramps and cycles, highlighting the sensitivity of AE to thermal loading.

Although much of the existing literature has focused on either the effects of thermal cycling or mechanical loading independently, the combined impact of these factors under confined in-situ stress conditions is less well understood. Confining pressure can impact the process of thermally induced microcracks and the ensuing variation in porosity and permeability. Furthermore, it is expected that thermal response of rocks would vary with textural characteristics which impact microcrack generation and AE signature.

In this work we investigate the thermo-mechanical response of the Utah FORGE granitoid. The effects of thermal cycling on triaxially loaded granitoid core plugs are studies using continuous dynamic measurements and AE monitoring. By subjecting the rocks to multiple heating and cooling cycles at varying peak temperatures, while continuously monitoring AE activity and dynamic properties, this research improves the understanding of microcrack development and propagation during thermal cycling under in-situ stress conditions. The

findings have practical applications for improving core-based stress measurement techniques, log interpretations and the design of thermal stimulation strategies.

2. METHODOLOGY

2.1 Sample Preparation

The granitoid rock at the depth of approximately 2,500 m within the Utah FORGE geothermal site is typically classified as a quartz monzodiorite or quartz diorite (Jones et al., 2024). Based on XRD analyses performed at EGI on a Bruker D-8 Advance XRD system (Jones et al., 2019), the mineral composition predominantly includes quartz, potassium feldspar, plagioclase, and biotite, with minor amounts of accessory minerals such as chlorite, epidote, and opaque minerals. The rock exhibits hypidiomorphic granular texture, where most crystals are partly euhedral (well-formed with distinct boundaries) to anhedral (poorly-formed). Hydrothermal alteration is present, particularly near fracture zones, with biotite often altered to chlorite, and feldspars displaying sericitization. The rock contains a well-developed network of microfractures, many associated with quartz and mica boundaries, attributed to thermal stress and tectonic activity. These features contribute to its permeability, which is crucial for enhanced geothermal system (EGS) operations.

Especially, the tested sample is retrieved from a depth of 8523 ft of Well 78-32. Its image and thin section are shown in Figure 1. Its basic information and minerology are summarized in Table 1 and 2, respectively. Its quartz composition is lower than expected from a typical granitoid, indicating dilution by secondary minerals.

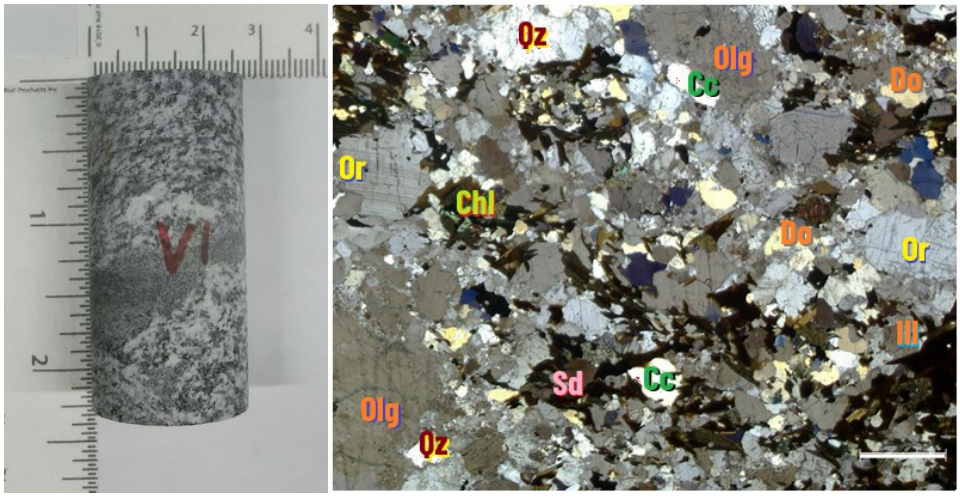

Figure 1: Sample image (left) and thin section (right white bar length is 1 mm).

Table 1: Sample information.

Well ID	Sample No.	Depth (ft)	Depth (m)	Length (mm)	Diameter (mm)	Weight (g)	Density (g/cm^3)	Hardness
78-32	V1	8523	2598	52.86	25.26	74.64	2.82	721

This sample's mineralogy by FTIR test is summarized in Table 2.

Table 2: Sample mineralogy in percent.

Quartz	Calcite	Dolomite	Illite	Smectite	Chlorite	Orthoclase	Oligoclase	Siderite
14	8	6	20	3	3	4	40	2

Note the high proportion of plagioclase feldspar (oligoclase), 40%, aligns with a granitoid's classification but suggests a more plagioclase-rich composition, which is consistent with quartz monzonite. The presence of 20% illite is unusual for an unaltered granitoid, suggesting significant alteration or secondary processes, such as hydrothermal activity or weathering. The presence of calcite, dolomite, and siderite totaling 16% indicates secondary mineralization from hydrothermal interactions including chemical alteration. These carbonates are not primary minerals in granitoids. This composition is consistent with a granitoid that has been subjected to hydrothermal fluid activity at

depth. The relatively low quartz content and the presence of significant secondary minerals like illite, smectite, chlorite, and carbonates indicate post-magmatic alteration. This aligns with the geothermal environment of Utah FORGE, where deep-seated rocks are altered by circulating hot fluids. The presence of clay minerals introduces unexpected complexities in the rock mechanical response of the sample.

The in-situ stress estimation is based on the understanding that the vertical stress (Sv) gradient is 1.13 psi/ft, the minimum horizontal stress (Sh) is 0.74 psi/ft, the maximum horizontal stress (SH) is in a range of 0.83 to 0.98 psi/ft, and pore pressure is 0.433 psi/ft (Ye et al., 2022). Based on these data, the effective mean stress at 8522ft depth is 3979 psi (using SH=0.83) to 4405 psi (using SH=0.98). In this test, we take the value of 4000 psi as the effective mean stress for this sample and use 2000 psi axial differential stress. For the temperature, based on the literature review, the reservoir temperature at this depth is in a range of 175 to 215ºC (Di Drill Survey, 2021), thus 180~ 190 ºC is taken as the in-situ temperature for this sample during the test.

2.2 Sample Installation

The rock sample preparation for triaxial testing starts by installing a copper jacket on the sample to fully encase the rock core. The copper sheet is cleaned with acetone to remove any contaminants, such as dirt or oils. Epoxy is used to seal any interfaces between the copper jacket and the platens, ensuring a secure secondary seal while also affixing the sample to the platens. After curing for about 24 hours, the sample pre-compressed under a confining pressure of 1000 psi to ensure the copper jacket tightly adheres to the rock surface. After that, linear variable displacement transducers (LVDTs) are attached to the sample for the measurement of strain. Finally, the sample is placed in the triaxial chamber, ensuring a snug fit to prevent any movement during testing (Figure 2).

Figure 2: Sample in copper jacket (left) and in the cell (right).

Before closing the triaxial cell, it is ensured that all signal wires are securely connected, including those for the LVDTs and a pair of piezoelectric transducers mounted on the platens for acoustic emission (AE) and Vp/Vs measurements. The experiment is conducted using an MTS 810 testing frame, which has a maximum axial load capacity of 250 kN, equivalent to 493 MPa on a 1-inch diameter sample. Control and data acquisition are managed through MTS Series 793™ Control software. Axial displacement of the rock sample is monitored using two LVDT sensors mounted on the sample, while a third LVDT attached to a radial chain measures transverse displacement with an associated error of ±0.05%. Temperature is regulated by a heating element around the cell, with a thermocouple installed inside the chamber to provide real-time temperature readings. Mechanical parameter measurements, including displacement and stress, are recorded throughout the loading process to evaluate the thermo-mechanical coupling behavior of the rock sample (Figure 3).

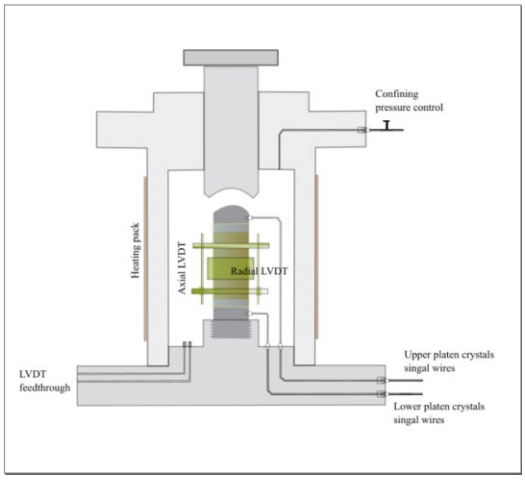

Figure 3: Schematic testing configuration.

2.3 Test Procedure

This test is divided into three main phases: (1) Stress Application, (2) Heating-Cooling Cycling, and (3) Triaxial Multistage Test.

Part 1: Stress Application at Room Temperature.

1. Install the rock sample into the cell and verify the signal quality of the LVDTs and acoustic sensors. Only proceed if the signals are acceptable.
2. Close the cell, fill it with mineral oil, and apply an initial confining pressure of 10 psi. Measure the compressional (Vp) and shear wave velocities (Vs).
3. Increase the confining pressure linearly from 10 psi to 1000 psi over 20 minutes, recording acoustic emission (AE) activity and LVDT displacement responses.
4. Hold the confining pressure at 1000 psi and measure Vp and Vs.
5. Gradually increase the confining pressure from 1000 psi to 2000 psi over 20 minutes, recording AE activity, LVDT responses, and bulk modulus changes.
6. Hold the confining pressure at 2000 psi and record Vp and Vs.
7. Repeat steps 5–6, increasing the confining pressure incrementally by 1000 psi until reaching 6000 psi. After recording Vp and Vs at 6000 psi, reduce the confining pressure to 4000 psi.
8. Maintain the confining pressure at 4000 psi, then increase the axial differential stress to 2000 psi. Record AE activity during this loading phase and measure Vp and Vs under these stress conditions, simulating in-situ stress for the sample.

Part 2: Acoustic Emission During Temperature Cycling.

9. Maintain a confining pressure of 4000 psi and an axial differential stress of 2000 psi. Gradually heat the sample from room temperature (25°C) to 60°C at a rate of 0.33°C/min, recording AE activity throughout the heating process.
10. Allow the sample to cool back to room temperature, recording AE activity during the cooling phase.
11. Conduct additional heating-cooling cycles: raise the temperature to 90°C and then cool to 30°C, recording LVDT responses, Vp/Vs, and AE signals.
12. Repeat the cycle in Step 11 for maximum temperatures of 120°C, 150°C, and 180°C, completing a total of five cycles. The procedure involves heating the sample during the daytime and allowing it to cool down overnight. This schedule ensures sufficient time for controlled heating and natural cooling, enabling accurate monitoring of the rock's thermal and mechanical responses in each cycle. Based on calculations, the cell temperature is a reliable indicator of the sample's temperature. Given the slow heating rate of 0.33°C/min and the system's high thermal conductivity, the temperature at the center of the granite rock closely aligns with the oil temperature near the wall, ensuring accurate monitoring.

Part 3: Triaxial Multistage Test at 180°C

13. At a constant temperature of 180°C, perform a multistage triaxial compression test starting with a confining pressure of 4000 psi. Use a loading rate of 1×10^{-3} mm/s (adjust if necessary) and unload the sample at the dilation point. Repeat the test at confining pressures of 3000 psi and 5000 psi, unloading at the dilation point for each stage.
14. For the final stage, return the confining pressure to 4000 psi and perform a triaxial compression test, continuing to load until the sample fails.
15. Cool the sample back to room temperature and complete the test. Remove the sample, document its condition with photographs, and clear the test station.

This structured methodology ensures the thorough characterization of the thermo-mechanical and acoustic responses of the sample under controlled laboratory conditions.

3. TEST RESULTS

3.1 Dynamic Properties and AE Behavior During Stress Application

The rock's dynamic properties and initial acoustic emission (AE) behavior were obtained during the first phase, referred to as the stress installation stage. The dynamic test results for the Utah FORGE rock reveal a clear relationship between effective stress and the rock's mechanical properties (Table 3 and Figure 4). As effective confining stress increases from 0.34 MPa to 41.37 MPa (50 to 6000 psi), the compressional wave velocity (Vp) and shear wave velocity (Vs) consistently rise, reaching values of 5182.35 m/s and 2753.13 m/s, respectively. This increase in wave velocities reflects the rock's densification and reduction in pore/microcrack space under higher stresses, enhancing its stiffness. Correspondingly, the dynamic Young's modulus (Ed) shows a steady increase from 33.27 GPa at low stress to 55.67 GPa at the highest confining pressure, indicating significant improvement in the rock's ability to resist deformation as confining pressure increases. The dynamic Poisson's ratio shows a gradual increase from 0.24 to 0.30, indicating a shift in the rock's elastic response under stress, with greater lateral deformation relative to axial deformation, suggesting less compressibility. These changes cumulatively reflect the rock's enhanced mechanical characteristics when subjected to increased confining pressures. Overall, increasing the confining pressure increases the stiffness of the rock by closing microcracks and voids, resulting in increased Young's moduli, bulk and shear moduli.

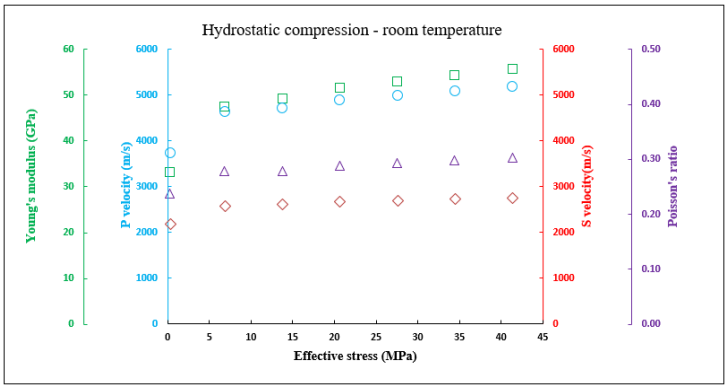

Figure 4: Dynamic test results under room temperature with increased effective stress.

Table 3: Dynamic test results at room temperature.

Effective stress (MPa)	Effective stress (psi)	Vp (m/s)	Vs (m/s)	Ed (GPa)	Dynamic Poisson's ratio
0.34	50	3722.54	2184.30	33.27	0.24
6.90	1000	4636.84	2566.02	47.47	0.28
13.79	2000	4719.64	2616.83	49.32	0.28
20.69	3000	4894.44	2669.70	51.74	0.29
27.58	4000	4986.79	2696.94	53.01	0.29
34.48	5000	5082.69	2724.74	54.32	0.30
41.37	6000	5182.35	2753.13	55.67	0.30

When the confining pressure increased prior to the application of axial differential stress, acoustic emission (AE) activity remained quiet. However, AE activity took off as soon as the piston made contact with the sample's top surface and the axial differential stress began to increase. This marked increase in AE activity with the application of differential stress loading contrasts with the relatively quiet period of confining pressure application. The observed behavior is clearly demonstrated by a strong correlation between the increase in deviatoric loading (and axial strain) which contributes to microcracking and the rise in AE activity (Figure 5).

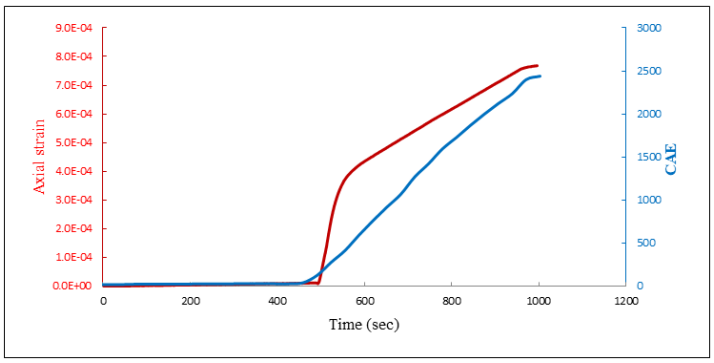

Figure 5: Correlation between axial strain and acoustic emission (AE) activity during axial differential stress loading.

3.2 Acoustic Emission and Deformation Behavior During Thermal Cycling

Under a constant stress boundary condition of 4000 psi confining pressure and an axial differential stress of 2000 psi, thermal cycling was conducted. This part of the test spanned approximately 3.88×10^5 seconds (about 4.5 days). Heating was performed at a controlled rate of 0.33°C/min, slow enough to ensure thermal equilibrium within the system. Cooling, on the other hand, occurred naturally at an even

slower rate. The five thermal cycles corresponded to target temperatures of 60°C, 90°C, 120°C, 150°C, and 180°C, with distinct heating and cooling phases as shown in the lower portion of Figure 6.

During thermal cycling, the deformation of the rock sample was predominantly axial, with minimal lateral strain. Axial strain and acoustic emission (AE) activities are illustrated in the upper portion of Figure 6. Specifically, the filtered (to eliminate noise) cumulative acoustic emission (CAE) closely mirrored the axial strain behavior. When the axial strain changed, the CAE exhibited a corresponding rise. When axial strain plateaued, AE activity stabilized accordingly.

During these thermal cycles, the axial shortening during the heating stages of 60°C, 90°C, 120°C, and 150°C, indicates progressive compaction. This behavior contrasts with the expected thermal expansion based on the granite's thermal expansion coefficient, which would typically result in elongation (strain decrease). The observed compaction suggests that thermally activated deformation mechanisms such as dislocation glide, grain boundary sliding, or microcrack closure may be dominant, leading to inelastic shortening of the sample under differential stress. However, at the heating stage of 180°C, the strain decreased, possibly reflecting the onset of thermal expansion overcoming the compaction effect or a reduction in creep activity as the creeping effect diminishes after sample became more consolidated.

During the cooling phases, the strain remained constant during cooling from 60°C to room temperature (RT), from 90°C to RT, and from 120°C to RT, suggesting that the compaction observed during heating was not reversible and no further deformation occurred during cooling. However, during the cooling phases from 150°C to RT and 180°C to RT, the strain increased, indicating additional compaction. This behavior may result from thermally induced stress redistribution or further microcrack closure as the temperature decreased, particularly under the influence of the newly increased temperature and the applied triaxial stress. These observations underscore the intricate interplay between thermal expansion, thermal-stress-driven compaction, and temperature-dependent deformation mechanisms in controlling the granite's response under cyclic thermal loading.

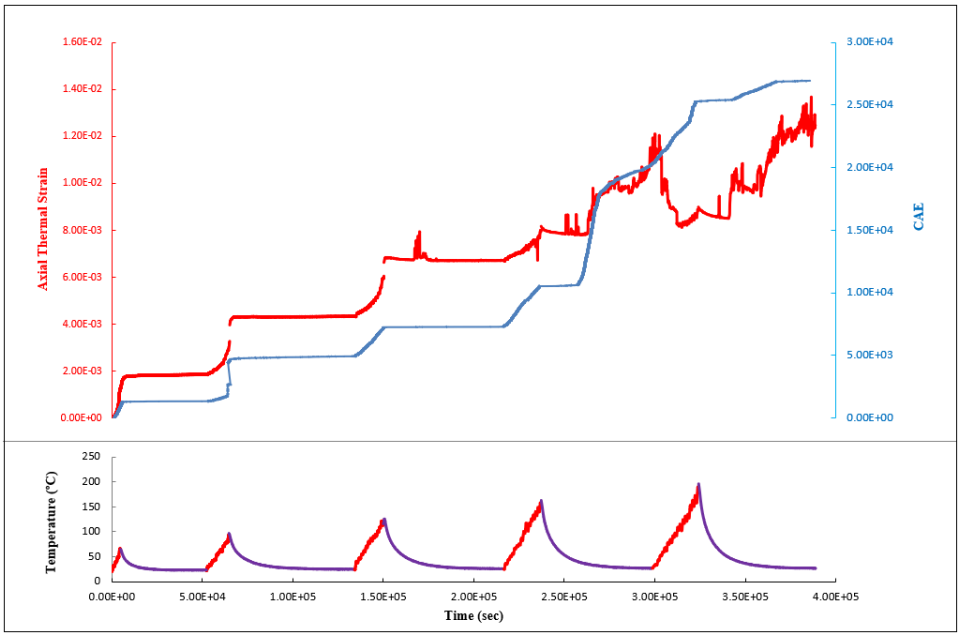

Figure 6: Temperature, axial thermal strain and CAE over time.

During the cooling phases after reaching 150°C, AE activity exhibited a pronounced surge, deviating from the quiet behavior observed in the first three cooling cycles. This surge in AE activity coincided with an increase and fluctuation in axial strain, indicating compaction of the rock. In the initial three thermal cycles, AE activity—a proxy for thermal crack development—was predominantly associated with the heating phases, while cooling phases exhibited minimal AE activity. However, in the last two cycles (cooling from 150°C to 25°C and 180°C to 25°C), AE activity significantly intensified. The surge during the first cooling phase (150°C–25°C) was notably stronger than the second (180°C–25°C), since new cracking requires surpassing previously experienced thermal paths. This behavior can be interpreted as a form of the thermal Kaiser effect.

These AE surges were consistently accompanied by axial strain fluctuations, indicating that thermal cracks induced during cooling contributed to measurable changes in the rock's geometry. The shift in behavior during cooling phases highlights a transition in the rock's response to thermal stress. These findings align with the observations of Daoud et al. (2020), who also reported AE surges during cooling phases. Their work demonstrated that thermal cracking predominantly occurs during heating in coarse-grained granophyre but shifts to occur during cooling in finer-grained andesite and basalt. Notably, the rock tested in this study exhibits a mixed grain structure, consisting of both coarse and fine grains (Figure 1), or a bimodal texture, which may potentially contribute to the observed behavior.

3.3 Dynamic Properties During Thermal Cycling

Compression and shear wave velocities have also been measured during thermal cycling. The dynamic test results of the Utah FORGE rock, while maintaining consistent stress boundary conditions with 4000 psi confining pressure and 2000 psi axial differential stress, reveal a clear temperature-dependent degradation of the rock's elastic properties (Table 4 and Figure 7). Initially at room temperature (25°C), the compressional wave velocity (Vp) and shear wave velocity (Vs) are highest, at 5286.00 m/s and 2841.94 m/s, respectively, correlating with a high dynamic Young's modulus (Ed) of 59.02 GPa and a dynamic Poisson's ratio of 0.29. As the temperature increases over cycling, both Vp and Vs decline, with Vp showing a more pronounced decrease. By 180°C, Vp has dropped to 4556.90 m/s, Vs to 2381.08 m/s, and the Young's modulus to 42.92 GPa, representing a substantial reduction in stiffness and wave propagation capacity.

Table 4: Dynamic results during thermal cycling.

Temperature	Vp	Vs	Ed	Dynamic Poisson's ratio	K	S
(°C)	(m/sec)	(m/sec)	(GPa)		(GPa)	(GPa)
25	5286.00	2841.93	59.01	0.29	48.39	22.76
60	5182.35	2872.82	59.44	0.27	44.67	23.25
25	4986.79	2811.70	56.44	0.26	40.37	22.28
90	5182.35	2782.10	56.59	0.29	46.59	21.81
25	4986.79	2811.70	56.44	0.26	40.37	22.28
120	5082.69	2566.01	49.31	0.32	48.05	18.55
25	5182.35	2811.70	57.53	0.29	45.97	22.28
150	4894.44	2470.09	45.69	0.32	44.58	17.19
25	5082.69	2782.10	56.09	0.28	43.71	21.81
180	4556.89	2381.08	41.92	0.31	37.21	15.97
25	5082.69	2782.10	56.09	0.28	43.71	21.81

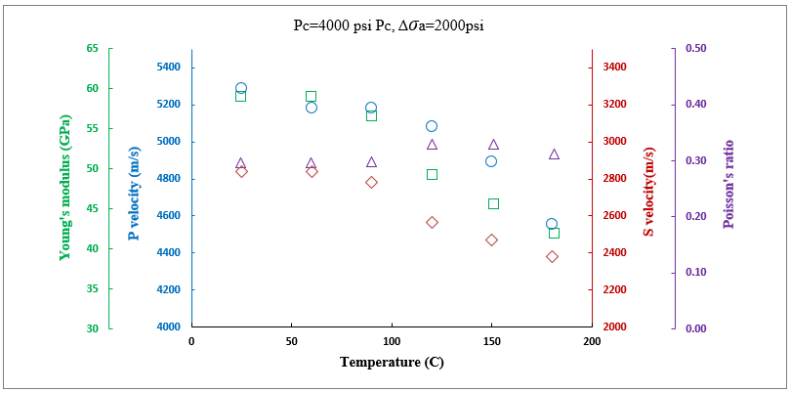

Figure 7: Dynamic test results under constant stress boundary conditions with increased temperature.

The observed trends underscore the thermal sensitivity of the rock, likely due to microstructural changes such as thermal expansion, crack initiation, and changes in mineral bonding strength. The shear wave velocity (Vs) displayed a monotonic decrease with increasing temperature. Thus, the shear modulus (calculated by $G = \rho Vs^2$), also diminished. A decreasing shear modulus usually indicates that the rock sample becomes progressively softer over the heating-cooling cycle.

After each cooling phase, the rock strength appears to recover partially, as indicated by the reversely increased Vp and Vs measured under room temperature. This recovery may result from the closing of some thermally induced microcracks due to contraction during cooling, stress redistribution, or structural realignments within the rock. Additionally, the presence of clays could play a role in this process, as their plasticity and potential to swell or contract with temperature changes may contribute to closing or aligning microcracks.

Comparing the final dynamic Young's modulus (Ed) at 180°C (41.92 GPa) with that at room temperature (59.01 GPa initially and 56.09 GPa after the last cooling cycle) shows a significant reduction in stiffness with increasing temperature, indicating irreversible thermal damage despite partial recovery after cooling. Comparing the strength data between room temperature and elevated temperatures would provide greater confidence in the results and offer deeper insights into the extent of structural changes occurring within the rock during thermal cycles.

3.4 Multistage test at 180°C

After the thermal cycling test, the temperature was raised to 180°C and maintained consistently, while a multistage test was conducted on the rock. Despite experiencing some thermal damage from the previous cycling, the rock retained significant strength.

During the multistage loading test, confining pressures of 4000, 3000, and 5000 psi were applied sequentially, with axial load increased to the dilation point in each stage before unloading. The dilation point is identified by monitoring the behavior of the volumetric strain curve, specifically when the tangent line of this curve begins to approach a vertical orientation. In the final stage with the confining pressure returned to 4000 psi, the axial load was applied to failure. The stress-strain behavior showed nonlinear elasticity during initial loading for each stage, as microcracks formed by differential thermal expansion closed under pressure, increasing stiffness. In the final stage, rapid and violent crack propagation led to failure, with a significant drop in residual stress. Elevated temperature and pressure activated deformation mechanisms such as grain boundary sliding and crystal plasticity, facilitating plastic deformation prior to failure. A well-developed shear fracture was evident, as marked on the copper jacket (Figure 8).

Figure 8: Distinct trace of a well-developed shear fracture marked on the copper jacket after rock failure.

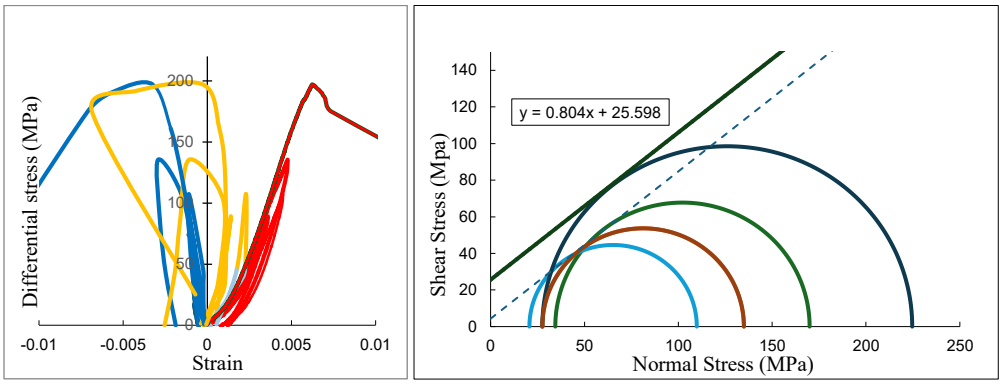

Figure 9: Stress-strain curve (left) and Mohr Coulomb analysis (right) of the multistage test.

Overall, this rock exhibits an intermediate Young's modulus and compressive strength, likely due to its texture and mineral composition. There is a strong correlation between the static and dynamic moduli, as well as Poisson's ratio. Both static and dynamic moduli decrease with increasing temperature (Table 5). At a 4000psi confining pressure, static Young's modulus was measured under room temperature and 180°C conditions, showing a reduction in both static and dynamic moduli with higher temperature.

Table 5: Variation of elastic and Poisson's ratio during multistage test.

Temperature (°C)	Pc (psi)	Es (GPa)	Static Poisson's ratio
180	3000	42.91	0.21
180	4000	42.27	0.24
180	5000	46.17	0.30
180	4000 (failure)	42.16	0.31

The comparison of static and dynamic Young's moduli at room temperature (25°C) and elevated temperature (180°C) reveals notable differences and trends (Table 6). Initially, at 25°C and a confining pressure of 4000 psi, the static Young's modulus (48.33 GPa) is significantly lower than the dynamic modulus (59.02 GPa). This difference likely reflects the influence of horizontal fissures and microcracks within this vertical sample, which could usually be caused by the core retrieving process due to the release of overburden stress. Such horizontal fissures typically have a more pronounced impact on static measurements than on dynamic ones. After multiple thermal cycles, both moduli exhibit a noticeable decrease with increasing temperature, indicating thermal damage to the rock. However, although the sample experienced overall thermal damage, its structure appears to compact over several days' triaxial stress conditions due to compaction effect, resulting in a smaller difference between the static (42.27 GPa) and dynamic (42.92 GPa) moduli at 180°C.

Table 6: Variation of elastic and Poisson's ratio during multistage test.

Temperature	Pc (psi)	Static E (GPa)	Dynamic E (GPa)
25	4000	48.33	59.02
180	4000	42.27	42.92

3.5 Thermal Kaiser Effect

In this experiment, we also observed variations in cumulative acoustic emission (CAE) during the cooling phases at different peak temperatures, which provide insights into the potential manifestation of the Thermal Kaiser effect. After heating the rock to 150°C, a significant increase in CAE was detected during the cooling phase, indicating active microcrack initiation. In contrast, after heating to 180°C, although some CAE was still recorded, the magnitude of the response was much smaller. This reduction in CAE during the cooling phase at higher temperatures aligns with the Thermal Kaiser effect, suggesting that the material "remembers" its previous thermal damage history. The rock's microstructural and mechanical state at elevated temperatures likely plays a crucial role in shaping its behavior during cooling, reducing the reactivation of pre-existing cracks and influencing the overall thermal damage progression.

The Thermal Kaiser effect has broader implications for understanding how rocks behave under cyclic thermal stress. This effect proposes that pre-existing thermal damage influences the material's response to subsequent heating and cooling, leading to a diminished acoustic response and slower mechanical degradation. As the rock undergoes repeated thermal cycling, its microstructure stabilizes, which can reduce the propagation of microcracks and slow the rate of thermal damage. These findings underscore the complex interplay between thermal history, crack evolution, and the material's long-term behavior, highlighting the importance of considering temperature memory when assessing the durability of rocks in geothermal environments.

4. DISCUSSION

The experimental results provide a comprehensive understanding of the thermo-mechanical behavior of granitoid cores from the Utah FORGE site under simulated geothermal reservoir conditions. The dynamic properties of the rock sample at room temperature reveal that increasing effective stress significantly enhances the rock's stiffness, which is evidenced by higher compressional (Vp) and shear wave (Vs) velocities, along with an increase in the dynamic Young's modulus (Ed). These changes are attributed to the closure of microcracks and voids under elevated confining pressures, highlighting the rock's potential to maintain mechanical integrity under the in-situ stress conditions typical of geothermal reservoirs.

Thermal cracking in rocks involves complex interactions during both heating and cooling phases. In our thermal cycling tests on the Forge 8523 ft core, cumulative acoustic emission (CAE) closely mirrored axial strain behavior, reflecting the rock's macro-scale deformation driven by internal micro-scale grain rearrangement and microcrack activities, including crack initiation, propagation, and closure. Notably, CAE increased during changes in axial strain and plateaued when strain stabilized. Acoustic emissions (AEs) were detected throughout all five heating phases and the final two cooling phases.

AEs caused by heating have been widely documented (Fortin et al., 2006; Griffiths et al., 2016, 2024; Jones et al., 1997), with the mechanism being relatively straightforward due to microcrack initiation caused by grain expansion. More recently, studies have highlighted that AEs during cooling, often attributed to thermal cooling microcracks, can be as significant as those observed during heating (Browning et al., 2016; Heap, 2014; Daoud, 2020). For example, Browning et al. (2016) observed that the vast majority of AE energy results from thermal cracking generated during the cooling phase rather than during the heating phase, and these findings underscore the significance of the cooling phase in thermal cracking studies, as it may contribute more substantially to rock damage than previously recognized. However, the physical mechanisms driving thermal damage-related AE during cooling remain complex and not fully understood. This complexity involves factors such as anisotropy, heterogeneity, pre-existing structural defects, thermal gradients, and heating history (Zhang et al., 2020).

In the research by Daoud et al. (2020), coarse-grained granophyre predominantly exhibited thermal crack damage during heating, whereas finer-grained andesite and basalt experienced more damage during cooling. Therefore, the bi-modal texture of the FORGE core tested may contribute to microcracking during both heating and cooling thermal phases, highlighting the complex nature of thermal cracking.

The absence of AE activity during the initial three cooling phases, followed by its emergence in the last two, suggests that heating beyond 15 °C may signify thermal Kaiser effect and the activation of specific mechanisms leading to AE during subsequent cooling phases. However, relying solely on AE monitoring to assess microstructural changes may be insufficient. Griffiths et al. (2018) combined AE monitoring with velocity measurements during thermal cycling of Westerly granite (not loaded) and found that many AEs recorded during cooling might not be associated with the formation of new microcracks but rather with the closing of existing ones. This indicates that AE activity during cooling may not always signify damage but could also represent microcrack closure, akin to the sounds heard both when a door opens (crack initiation/propagation) and closes (crack sealing). In our case, we also observed that partially recovered Vp/Vs after cooling suggests that crack closure, accompanied by AE activity, might also be occurring. If this is the mechanism, the quiet cooling phases in the first three cycles may indicate that cracks produced during the previous heating processes sealed quietly, while further heating at higher temperatures may have triggered more thermal stress driven cracks, causing energy release when such cracks begin to seal.

The disparity in damage observed between the heating and cooling phases may also be attributed to changes in the overall stress state within the sample. Materials typically have a tensile strength that is approximately one-tenth of their compressive strength. As a result, cracks are more likely to form under the tensile stresses induced by cooling and contraction than under the compressive stresses associated with heating and expansion. In our test, although the confining pressure and axial stress maintained a compressive regime throughout, the transition from grain expansion during heating to contraction during cooling likely caused complex stress redistributions. These redistributions may have locally favored the formation of microcracks during the cooling phase. This process highlights how the interplay between thermal expansion, contraction, and stress state can influence microstructural damage evolution.

Studies by Heap et al. (2014) have documented varying AE activity during heating and cooling across different rock types (unstressed), with AE during cooling often attributed to thermal contraction or crack interactions. Since cooling always occurred after heating, the previous crack formation may have impacted the subsequent crack behavior, either with new cracks further developing or old crack being sealed somehow. Therefore, integrating AE monitoring with complementary techniques, such as velocity or permeability measurements, is essential for a comprehensive understanding of thermal damage mechanisms in rocks. This multifaceted approach enables a more accurate interpretation of AE data, distinguishing between crack formation, closure, and sealing processes during thermal cycling.

Furthermore, the unique mineralogical composition of the Utah FORGE rock, characterized by a high proportion of oligoclase and secondary minerals such as illite and carbonates, likely contributes to its distinct thermo-mechanical response. These secondary minerals, products of hydrothermal alteration, may weaken the rock matrix, making it more susceptible to damage under thermal cycling. This finding highlights the importance of considering mineralogical heterogeneity in geothermal reservoir characterization.

5. CONCLUSION

This study underscores the critical role of thermal cycling in altering the mechanical and microstructural properties of granitoid rocks under in-situ geothermal conditions. The experimental results highlight the following key findings:

Acoustic emission (AE) activity remained minimal during hydrostatic loading but surged significantly once axial differential stress was applied. The strong correlation between AE activity and axial thermal strain under a constant stress boundary condition is evident throughout all subsequent thermal cycles. Since cumulative acoustic emission (CAE) closely mirrored axial strain behavior, the rock's macro-scale deformation, driven by internal micro-scale grain rearrangement, can be effectively captured by analyzing AE, strain, and dynamic measurements.

AEs were detected during all five heating phases and the final two cooling phases. The mechanism of AE during heating is relatively straightforward, driven by microcrack initiation due to grain expansion/rearrangement. However, the mechanism of AE during cooling is more complex and difficult to interpret. The absence of AE activity during the initial three cooling phases, followed by its emergence in the final two, suggests that heating beyond 150°C may activate specific mechanisms leading to AE during subsequent cooling phases. The bimodal grain structure of the rock likely contributed to this behavior.

On the other hand, the partially recovered Vp/Vs after cooling further suggests that crack sealing, accompanied by AE activity, may also be occurring. If this is the case, the quiet cooling phases in the first three cycles may indicate that cracks produced during previous heating cycles sealed quietly, while further heating at higher temperatures may trigger more rigid cracks, leading to energy release when these cracks begin to seal. However, the physical mechanisms driving thermal related AE during cooling remain complex and not fully

understood. These complexities involve factors such as anisotropy, heterogeneity, pre-existing structural defects, and thermal history. Our work provides valuable observations for further investigation into these phenomena.

Overall, repeated heating and cooling cycles induce significant and cumulative microcrack damage, as evidenced by notable axial deformation, AE activity, and reduced Vp/Vs. The damage progressively accumulates with each cycle, particularly at higher peak temperatures. The interplay between thermal damage and mechanical stress plays a crucial role in influencing the rock's failure mechanisms. Multistage triaxial tests reveal that both the dilation point and fracture propagation are sensitive to confining pressure and prior thermal cycling.

The observed variations in cumulative acoustic emission (CAE) during cooling phases at different peak temperatures also suggest the presence of the Thermal Kaiser effect, indicating that the rock "remembers" its thermal history, which influences its subsequent acoustic response. These findings highlight the role of pre-existing thermal damage in shaping the rock's mechanical degradation and emphasize the importance of considering thermal memory in assessing the long-term durability of rocks under cyclic thermal stress.

The presence of secondary minerals, such as illite and carbonates, weakens the rock matrix, likely amplifying the effects of thermal cycling on mechanical properties. These minerals contribute to the rock’s vulnerability to thermal damage, affecting its overall strength and response to thermal cycling.

Together, these results emphasize the intricate interplay between thermal cycling, thermal memory (thermal Kaise effect), grain structure, and the evolution of thermal cracks in thermally stressed rocks, underscoring the complexity of thermal damage mechanisms in heterogeneous materials. These findings have important implications for the design and optimization of Enhanced Geothermal Systems (EGS).

REFERENCES

Allis, R., Gwynn, M., Hardwick, C., Hurlbut, W., Kirby, S.M., and Moore, J.N., 2019, Thermal characteristics of the Roosevelt Hot Springs system, with focus on the FORGE EGS site, Milford, Utah, in Allis, R., and Moore, J.N., editors, Geothermal characteristics of the Roosevelt Hot Springs system and adjacent FORGE EGS site, Milford, Utah: Utah Geological Survey Miscellaneous Publication 169-D, 22 p., https://doi.org/10.34191/MP-169-D.

Browning, J., Meredith, P., Gudmundsson, A., 2016. Cooling-dominated cracking in thermally stressed volcanic rocks. Geophysical Research Letters, 43(16), 8425. https://doi.org/10.1002/2016GL070532.

Bu, M., Guo, P., Jin, X., Wang, M., Zhang, P., Wang, J., 2024. Temperature-dependent acoustic emission characteristics and statistical constitutive model of granite under uniaxial compression, Journal of Rock Mechanics and Geotechnical Engineering, ISSN 1674-7755, https://doi.org/10.1016/j.jrmge.2024.05.033.

Chen, S., Yang, C., Wang, G., 2017. Evolution of thermal damage and permeability of Beishan granite. Applied Thermal Engineering, Volume 110, Pages 1533-1542, ISSN 1359-4311, https://doi.org/10.1016/j.applthermaleng.2016.09.075.

Darot, M., Gueguen, Y., Baratin, M-L., 1992. Permeability of thermally cracked granite. Geophysical Research Letters, Vol 19 (9), 869-872.

David, C., Menéndez, B., Darot, M., 1999. Influence of stress-induced and thermal cracking on physical properties and microstructure of La Peyratte granite. International Journal of Rock Mechanics and Mining Sciences, Volume 36, Issue 4, Pages 433-448, ISSN 1365-1609, https://doi.org/10.1016/S0148-9062(99)00010-8.

Di Drill Survey Services., 2021. Utah FORGE: Wells Updated Temperature and Pressure Logs (June 2021) [data set]. Retrieved from https://dx.doi.org/10.15121/1812334.

Daoud, A., Browning, J., Meredith,P. G., Mitchell, T. M., 2020. Microstructural controls on thermal crack damage and the presence of a temperature-memory effect during cyclic thermal stressing of rocks. Geophysical Research Letters, 47, e2020GL088693. https://doi.org/10.1029/2020GL088693.

Fortin, J., Stanchits, S., Dresen, G., & Guéguen, Y., 2006. Acoustic emission and velocities associated with the formation of compaction bands in sandstone. Journal of Geophysical Research, 111(B10), B10203. https://doi.org/10.1029/2005jb003854.

Fredrich, JT., Wong, TF., 1986. Micromechanics of thermally induced cracking in three crustal rocks. J Geophys Res. Solid Earth 91(B12):12743–12764. https://doi.org/10.1029/JB091iB12p12743

Ge, Z., Sun, Q., 2018. Acoustic emission (AE) characteristics of granite after heating and cooling cycles, Engineering Fracture Mechanics, Volume 200, Pages 418-429, ISSN 0013-7944, https://doi.org/10.1016/j.engfracmech.2018.08.011.

Ghassemi A. 2012. A review of some rock mechanics issues in geothermal reservoir development. Geotechnical and Geological Engineering 30(3), 647-664.

Griffiths, L., Lengliné, O., Heap, M. J., Baud, P., & Schmittbuhl, J., 2018. Thermal cracking in Westerly Granite monitored using direct wave velocity, coda wave interferometry, and acoustic emissions. Journal of Geophysical Research: Solid Earth, 123, 2246–2261. https://doi.org/10.1002/2017JB01519.

Griffiths, L., Heap, M. J., Lengliné, O.,Baud, P., Schmittbuhl, J., Gilg, H. A., 2024. Thermal stressing of volcanic rock: Microcracking and crack closure monitored through acoustic emission, ultrasonic velocity, and thermal expansion. Journal of Geophysical Research: SolidEarth, 129, e2023JB027766. https://doi.org/10.1029/2023JB027766.

Heap, M. J., Lavallée, Y., Petrakova, L., Baud, P., Reuschlé, T., Varley, N. R., Dingwell, D. B., 2014. Microstructural controls on the physical and mechanical properties of edifice-forming Andesites at Volcán de Colima, Mexico. Journal of Geophysical Research: Solid Earth, 119(4), 2963. https://doi.org/10.1002/2013JB010521.

Huang, K., Cheng, Q., Ghassemi, A., Bauer, A., 2019. Evaluation of shear slip in fractured rock using a 3D coupled thermo–poromechanical FEM. Int. J. Rock Mech. 120, 68-81.

Jin, P., Hu, Y., Shao, J., et al., 2019. Influence of different thermal cycling treatments on the physical, mechanical and transport properties of granite, Geothermics, Volume 78, Pages 118-128, ISSN 0375-6505, https://doi.org/10.1016/j.geothermics.2018.12.008.

Jones, C., Keaney, G., Meredith, P., Murrell, S., 1997. Acoustic emission and fluid permeability measurements on thermally cracked rocks. Physics and Chemistry of the Earth, 22(1), 13–17. https://doi.org/10.1016/S0079-1946(97)00071-2.

Jones, C.G., Moore, J.N., and Simmons, S., 2019, Petrography of the Utah FORGE site and environs, Beaver County, Utah, in Allis, R., and Moore, J.N., editors, Geothermal characteristics of the Roosevelt Hot Springs system and adjacent FORGE EGS site, Milford, Utah: Utah Geological Survey Miscellaneous Publication 169-K, 23 p., 2 appendices, https://doi.org/10.34191/MP-169-K.

Jones, C., Simmons, S., Moore, J., 2024. Geology of the Utah Frontier Observatory for Research in Geothermal Energy (FORGE) Enhanced Geothermal System (EGS) Site. Geothermics 122 (2024) 103054.

Lockner, D., Byerlee, J., Kuksenko, V., Ponomarev, A., Sidorin, A., 1991. Quasi-static fault growth and shear fracture energy in granite. Nature, 350(6313), 39-42.

Obert, L., 1977. The Microseismic Method: Discovery and Early history//Proceeding First Conference on Acoustic Emission / Microseismic Activity in Geologic Structures and Materials. Clausthal: Trans Tech Publications

Reuschle T, Haore SG, Darot M., 2006. The effect of heating on the microstructural evolution of La Peyratte granite deduced from acoustic velocity measurements. Earth Planet Sci Lett. 243(3-4):692–700.

Rong, G., Peng, J., Cai, M., Yao, M., Zhou, C., Sha, S., 2018. Experimental investigation of thermal cycling effect on physical and mechanical properties of bedrocks in geothermal fields, Applied Thermal Engineering, Volume 141, 2018, Pages 174-185, ISSN 1359-4311, https://doi.org/10.1016/j.applthermaleng.2018.05.126.

Tester, J. W., Drake, E. M., Richards, M., 2006. The Future of Geothermal Energy: Impact of Enhanced Geothermal Systems (EGS) on the United States in the 21st Century. Massachusetts Institute of Technology.

Wang, F., Frühwirt, T., Konietzky, H., 2020. Influence of repeated heating on physical-mechanical properties and damage evolution of granite. International Journal of Rock Mechanics and Mining Sciences, Volume 136, 2020, 104514, ISSN 1365-1609, https://doi.org/10.1016/j.ijrmms.2020.104514.

Wang, H. F., Bonner, B.P., Carlson S.R., Kowallis, B.J., Heard, H.C., 1989. Thermal Stress Cracking in granite, J. Geophys. Res., 94, 1745–1758, 1989

Ye, Z., Fang, Y., Ghassemi, A., McLennan, J., 2022. A Preliminary Wellbore In-situ Stress Model for Utah FORGE. ARMA US Rock Mechanics/Geomechanics Symposium, ARMA-2022-0272.

Ye, Z., Ghassemi, A. 2018. Injection-induced shear slip and permeability enhancement in granite fractures. J. Geoph. Res, Solid Earth, 123, 24 p.

Ye, Z., Ghassemi, A. 2019a. Injection-Induced Propagation and Coalescence of Preexisting Fractures in Granite Under Triaxial Stress. J. Geoph. Res, Solid Earth, 124, 16 p.

Ye, Z., Vachaparampil, A., Zhou, X., Ghassemi, A., Kneafsey, T. 2019b. Failure behavior of the Poorman schist and its fractures from EGS collab stimulation site. 44th workshop on geothermal reservoir engineering, Stanford University, Stanford, California, February 11-13, 2019, SGP-TR-214.

Ye, Z., Ghassemi, A. 2020. Heterogeneous fracture slip and aseismic-seismic transition in a triaxial injection test. Geophysical Research Letters, 47(14), e2020GL087739.